A Collisional and Radiative Model of Argon Plasma for Application to Ionization Phenomena Behind a Shock Wave

By

Yasunari TAKANO* and Teruaki AKAMATSU*

(Received September 16, 1981)

Abstract

A formulation has been performed for the description of excited-level population-densities and gasdynamic properties in nonequilibrium ionizing argon gas. The energy-level structure of an argon atom is assumed to be composed of six actual levels and higher hydrogenic levels. The ionization and excitation due to atom-atom and atom-electron inelastic collisions, as well as radiative transition including the self-absorption effect, are considered in the model. Applying the collisional and radiative model, calculations have been made for the ionization phenomena of shock-heated argon gas. The results show that the ionization relaxation region behind a shock consists of initial ionization, induction, rapid ionizing and equilibrium parts. Also there are sharp peaks of lower excited-level population-densities in the initial ionization region. The simulations, carried out for line-intensity, show that the self-absorption in lines has a significant influence on line-intensity measurements.

Nomenclature

A_{ij} : bound-bound transition probability
A_{Ij} : free-bound transition probability
a_j : photo-ionization cross-section from *jth* level
a_0 : Bohr radius
B_{ij} : Einstein coefficient for absorption
c : speed of light
E : kinetic energy available for an inelastic collision
E_A : rate of energy loss of heavy particles compensated for excitation and ionization
E_B : rate of energy loss of electrons due to bremsstrahlung radiation
E_C : rate of energy loss of electrons due to radiative recombination
E_H : ionization energy of a hydrogen atom

* Department of Mechanical Engineering.

E_I : rate of energy loss of electrons due to atom-electron inelastic collisions
E_{ij} : excitation energy of i to j transition
E_j : ionization energy of *jth*-level atom
E_T : rate of energy transferred to electrons by heavy particles during elastic collisions
e : charge of an electron
f_{ij} : oscillator strength
g_j : statistical weight of *jth* level
$\bar{g}$: effective Gaunt factor
h : Plank constant
I_ν : radiative intensity
I_{ij} : line intensity
k : Boltzmann constant,
absorption coefficient including induced emission
K_{ij} : rate coefficient for excitation due to atom-atom collisions
K_{jI} : rate coefficient for ionization due to atom-atom collisions
L : line shape factor
m_a : mass of an atom
m_e : mass of an electron
m_H : mass of a hydrogen atom
n_a : number density of neutral atoms
n_e : number density of electrons
$\dot{n}_e$: electron production rate
n_j : number density of atoms in *jth* level
$\dot{n}_j$: production rate of *jth*-level atoms
p : pressure of plasma
Q_{ij} : cross-section for excitation
Q_{jI} : cross-section for ionization
Q_{ea} : elastic cross-section between electrons and atoms
Q_{ei} : elastic cross-section between electrons and ions
R : gas constant of plasma ($=\mathrm{k/m}_a$)
r_0 : effective radius of radiating plasma, radius of shock tube
S_{ij} : rate coefficient for excitation due to atom-electron collisions
S_{jI} : rate coefficient for ionization due to atom-electron collisions
T : temperature of heavy particles
T_e : electron temperature
u : velocity of plasma

v : velocity of an electron
x : distance from shock front
Z_I : partition function of ions
α : degree of ionization,
fine structure constant ($=1/137$)
β_{ij} : radiation escape factor for bound-bound transition
β_{Ij} : radiation escape factor for free-bound transition
Γ_{ij} : half width of Stark broadening
$\Delta\nu_d$: Doppler width
ε_A : rate of thermal energy given to ejected electrons by atom-atom ionizations
ν : frequency of light
ν_{ij} : line frequency
ν_{ea} : elastic collision frequency between electrons and atoms
ν_{ei} : elastic collision frequency between electrons and ions
ρ : mass density of plasma

1. Introduction

Many investigations have been made concerning the ionization relaxation process behind a strong shock in rare gas. In gas heated by shock, ionization initially takes place mainly due to atom-atom inelastic collisions and afterwards dominantly due to atom-electron inelastic collisions. When the atom-electron collisional ionization become dominant, the ionization proceeds rapidly toward equilibrium. Thus, the equilibration of the shocked gas requires an ionization relaxation time. After equilibration, a radiative-cooling effect appears as a decay of ionization degree in the ionized gas.

Petschek & Byron[1] performed a pioneering investigation on the mechanism of ionization in shock-heated argon. They noticed the excitation process to the first excited-state, instantaneously followed by ionization, controlling the ionization rate, and proposed a model of the two-step process for ionization approaching to equilibrium. For the initial ionization, Weymann[2] proposed a two-step model of atom-atom inelastic collisions. A number of investigations followed[3-7]. In these works, the two-step process for ionization was assumed, namely atoms are excited to the first excited-level and subsequent collisions ionize the excited atom instantaneously. Consequently, the excited levels are assumed to be always in thermodynamic equilibrium with free electrons in a nonequilibrium relaxation region.

De Boer & Grimwood[8] suggested that the initial ionization behind a shock front actually proceeds with more than two steps. They argued that the ladder-

climbing mechanism is most effective, in which atoms are successively and collisionally excited to the next higher level. Hollenbach & Salpeter[9] made an attempt to estimate the atom-atom ionization rate of argon, considering the ladder-climbing model, where the many excited-states are combined into some quasi-states. They proposed semi-empirical formulas for excitation and ionization rates. Kamimoto, Teshima & Nishimura[10] investigated the whole ionization relaxation zone behind a shock in argon, considering four excited quasi-states. They found that the lower three excited-states were overpopulated until the end of the equilibration. Wojciechawski & Weymann[11] used the model of Hollenbach & Salpeter for their investigation of the initial ionization.

On the other hand, in recent years, there has been considerable interest in the radiative and collisional process in non-equilibrium arc plasma flow. Giannaris & Incropera[12] formulated a rigorous model, based on the collisional and radiative model of Bates, Kingston & McWhirter[13], to determine the effect of electron collisions on excited-level population-densities. Shirai, Tabei & Kakinuma[14] also made theoretical and experimental investigations on excited-level population-densities in low-density argon arc plasma flows.

In the present study, a model is formulated to determine the excited-level population-densities of argon atoms in nonequilibrium plasma. In the model, argon atoms are assumed to have six actual states and higher hydrogenic states. We consider the contributions of atom-atom inelastic collisions as well as atom-electron inelastic collisions for excitation and ionization. For radiative transitions, the effects of the self-absorption in lines are estimated and simple formulas are proposed. By applying the model, calculations are made on flow properties and excited-level population-densities in the ionization relaxation region behind a strong shock in argon.

2. Gasdynamic Conservation Equations

Continuous descriptions of a nonequilibrium partially ionized gas have been given and discussed by Appleton & Bray[15] and Mitchner & Kruger[16]. In their formulations, the collisional-radiative mechanism due to inelastic collisions of electrons with atoms is included but the effects of atom-atom inelastic collisions are neglected. In the present study, we investigate the ionization relaxation phenomena behind a strong shock in argon, so that the inelastic collisions of atoms, which are important in the initial stage of ionization, are considered in the formulation.

For simplicity of the analyses, the following assumptions are introduced: (i) in a mixture of atoms, ions and electrons, each species has a near-Maxwellian distribution; (ii) the gas is singly ionized and the electron number-density is equal

to the ion number-density; (iii) the atom and ion temperature is equal, and atoms and ions have the same velocity; (iv) the effects of viscosity, thermal conduction and diffusion are neglected.

In a coordinate system travelling at the velocity of the shock front, the following set of time-independent, one-dimensional conservative relations can be applied:

(mass) $$\rho u = \rho_0 u_0 = \text{constant}, \tag{1}$$

(momentum) $$\rho u^2 + p = \rho_0 u_0^2 + p_0 = \text{constant}, \tag{2}$$

(kinetic energy of heavy particles)

$$\frac{d}{dx}\left(\frac{3}{2}\rho RTu\right) + \rho RT\frac{du}{dx} = -E_T - E_A - \varepsilon_A, \tag{3}$$

(electron density) $$\frac{d}{dx}(n_e u) = \dot{n}_e, \tag{4}$$

(kinetic energy of electrons)

$$\frac{d}{dx}\left(\frac{3}{2}n_e k T_e u\right) + n_e k T_e \frac{du}{dx} = E_T + \varepsilon_A - E_I - E_C - E_B. \tag{5}$$

The thermal equation of state can be expressed as

$$p = \rho R(T + \alpha T_e) \tag{6}$$

In addition, the conservation equation for n_j, the atom density in the *jth*-state, is written as

$$\frac{d}{dx}(n_j u) = \dot{n}_j. \tag{7}$$

As the relaxation time of excited atoms is much shorter than the ionization-relaxation time, the value n_j for $j>1$ tends to be in balance with the instantaneous values of n_e and n_1. Therefore,

$$\dot{n}_j = 0, \qquad j>1 \tag{8}$$

is set.

3. Collisional and Radiative Model

3.1 Rate equations

The rate of electron production $\dot{n}_e$ consists of the rate due to atom-atom inelastic collisions $(\dot{n}_e)_a$, the rate due to atom-electron inelastic collisions $(\dot{n}_e)_e$, and the rate due to radiative transitions $(\dot{n}_e)_r$:

$$\dot{n}_e = (\dot{n}_e)_a + (\dot{n}_e)_e + (\dot{n}_e)_r, \tag{9}$$

where

$$(\dot{n}_e)_a = n_a \sum_j (n_j K_{jI} - n_e^2 K_{Ij}) , \tag{10}$$

$$(\dot{n}_e)_e = n_e \sum_j (n_j S_{jI} - n_e^2 S_{Ij}) , \tag{11}$$

$$(\dot{n}_e)_r = -n_e^2 \sum_j A_{Ij}\beta_{Ij} . \tag{12}$$

The rate of *jth*-level atom production $\dot{n}_j$ can also be written in terms of atom-atom collisional rate $(\dot{n}_j)_a$, atom-electron collisional rate $(\dot{n}_j)_e$, and radiative transitional rate $(\dot{n}_j)_r$:

$$\dot{n}_j = (\dot{n}_j)_a + (\dot{n}_j)_e + (\dot{n}_j)_r , \tag{13}$$

where

$$(\dot{n}_j)_a = n_a\Big(\sum_{i\neq j} n_i K_{ij} - n_j \sum_{i\neq j} K_{ji} - n_j K_{jI} + n_e^2 K_{Ij}\Big) , \tag{14}$$

$$(\dot{n}_j)_e = n_e\Big(\sum_{i\neq j} n_i S_{ij} - n_j \sum_{i\neq j} S_{ji} - n_j S_{jI} + n_e^2 S_{Ij}\Big) , \tag{15}$$

$$(\dot{n}_j)_r = \sum_{i>j} n_i A_{ij}\beta_{ij} - n_j \sum_{i<j} A_{ji}\beta_{ji} + n_e^2 A_{Ij}\beta_{Ij} . \tag{16}$$

3.2 Energy Levels

In the present investigation, the system of energy levels of argon is assumed to be composed of six actual levels and higher hydrogenic levels, as listed in Table 1. For the five actual excited-states, the levels are coalesced according to common configurations, and the energy value of a coalesced level is the weighted-average value. For higher hydrogenic levels, the value of ionization energy is approximated to

$$E_j = E_H/n^2 , \tag{17}$$

where $n=j-3$ is the principal quantum number of the higher hydrogenic *jth* level.

Table 1. Energy level system of argon I

level number j	configuration	statistical weight g_j	ionization energy E_j (erg.)
1	$3p$	1	2.525×10^{-11}
2	$4s$	12	6.580×10^{-12}
3	$4p$	36	4.147×10^{-12}
4	$3d$	60	2.682×10^{-12}
5	$5s$	12	2.603×10^{-12}
6	$5p$	36	1.907×10^{-12}
7	$n=4$	192	1.345×10^{-12}
⋮	⋮	⋮	⋮
j	$n=j-3$	$12n^2$	E_H/n^2
⋮	⋮	⋮	⋮

$E_H=2.152\times10^{-11}$ erg.: ionization energy of hydrogen atom,
n: principal quantum number of hydrogenic level.

4. Collisional Rate Coefficients

4.1 Atom-Electron Inelastic Collisions

For excitation cross-section due to atom-electron inelastic collisions, the Bethe approximation gives the simple expression.

$$Q_{ij}(E) = \frac{8\pi^2}{\sqrt{3}} a_0^2 \frac{E_H}{E_{ij}} \frac{E_H}{E} f_{ij} \bar{g}\,, \tag{18}$$

(See Seaton[17].)

where f_{ij} is the oscillator strength and $\bar{g}$ the effective Gaunt factor. The rate coefficients can be written in terms of electron energy distribution $f(v)$, electron velocity $v=(2E/m_e)^{1/2}$ and the cross-section Q_{ij} as follows:

$$S_{ij} = \int_{v_{ij}}^{\infty} Q_{ij}\left(\frac{m_e v^2}{2}\right) v f(v)\, dv \tag{19}$$

$$v_{ij} = \left(\frac{2E_{ij}}{m_e}\right)^{1/2}.$$

With the assumption of the Maxwellian distribution for electron gas,

$$f(v) = 4\pi\left(\frac{m_e}{2\pi k T_e}\right)^{3/2} v^2 \exp\left(-\frac{m_e v^2}{2kT_e}\right), \tag{20}$$

$$S_{ij}(T_e) = \frac{8\pi^2}{\sqrt{3}} a_0^2 \frac{E_H}{kT_e} \frac{E_H}{E_{ij}} \left(\frac{8kT_e}{\pi m_e}\right)^{1/2} f_{ij} \exp\left(-\frac{E_{ij}}{kT_e}\right) P\left(\frac{E_{ij}}{kT_e}\right), \tag{21}$$

$$P(y) = \int_0^{\infty} \bar{g}(x) e^{-yx^2} d(yx^2) \tag{22}$$

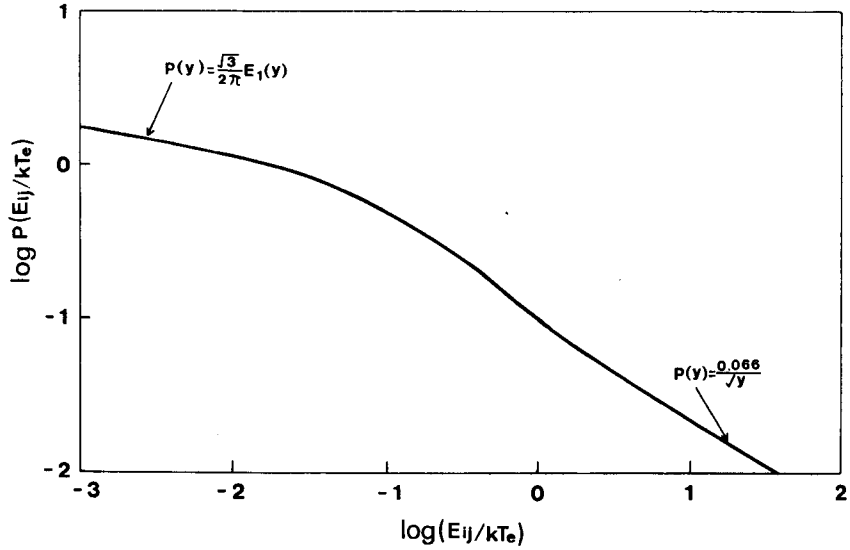

Fig. 1. Averaged Geaunt factor.

Table 2. Numerical values for collisional and radiative transions

i	j	$A_{ij}(s^{-1})$	f_{ji}	$\lambda_{ij}(\mu m)$	$\Gamma_{ij}/4\pi(s^{-1})$		
					(5000 K)	(10000 K)	(20000 K)
2 (4s)	1 (3p)	0.157E9	0.320	0.1064	0.481E-11	0.551E-11	0.578E-11
3 (4p)	2 (4s)	0.364E8	1.092	0.0816	0.413E- 9	0.553E- 9	0.741E- 9
4 (3d)	1 (3p)	0.292E8	0.203	0.0880	0.905E-11	0.112E-10	0.136E-10
4 (3d)	3 (4p)	0.111E8	0.507	1.3552	0.235E- 9	0.264E- 9	0.295E- 9
5 (5s)	1 (3p)	0.280E8	0.039	0.0887	0.234E-10	0.273E-10	0.282E-10
5 (5s)	3 (4p)	0.223E8	0.184	1.2858	0.472E- 8	0.579E- 8	0.685E- 8
6 (5p)	2 (4s)	0.124E7	0.010	0.4250	0.116E- 8	0.141E- 8	0.157E- 8
6 (5p)	4 (3d)	0.228E7	0.135	2.5623	0.286E- 7	0.350E- 7	0.404E- 7
6 (5p)	5 (5s)	0.415E7	1.520	2.8537	0.179E- 7	0.201E- 7	0.226E- 7
7 (n=4)	6 (5p)	0.992E6	1.487				
7 (n=4)	5 (5s)	0.259E6	0.105				
7 (n=4)	4 (3d)	0.602E7	0.571				
7 (n=4)	3 (4p)	0.649E6	0.041				
8 (n=5)	6 (5p)	0.133E6	0.060				
8 (n=5)	5 (5s)	0.137E6	0.055				
8 (n=5)	4 (3d)	0.127E7	0.103				
8 (n=5)	3 (4p)	0.493E6	0.023				
9 (n=6)	6 (5p)	0.103E5	0.041				

i, j: level number,
A_{ij}: radiative transition probability,
f_{ij}: oscillator strength,
λ_{ij}: wave length of coalesced line,
$\Gamma_{ij}/4\pi$: (half) half width of Stark broadening at the electron density $10^{16}\mathrm{cm}^{-3}$.
read, e.g. $0.157E9 = 0.157 \times 10^{9}$

is reduced. Regemotor[18] gave the values of $P(y)$ which are shown in Figure 1. The oscillator strengths used in the present study are listed in Table 2.

Seaton[17] showed the ionization cross-section as

$$Q_{ji}(E) = \frac{2}{\alpha\sqrt{3}} \frac{E_H}{E} \int_0^{E-E_j} \frac{a_j(E')\bar{g}}{E_j+E'} dE' , \tag{23}$$

where $a_j(E')$ is the photo-ionization cross-section from the j*th*-level with the kinetic energy E' of the ejected electron, and $\bar{g}$ the Gaunt factor. For near-threshold ionization, it reduces to

$$Q_{ji}(E) = \frac{2}{\alpha\sqrt{3}} a_j(0) \frac{E_H}{E} \frac{E-E_j}{E_j} \bar{g} . \tag{24}$$

The ionization rate coefficient can be deduced for the near-threshold ionization as

$$S_{ji}(T_e) = \frac{2}{\alpha\sqrt{3}} a_j(0) \left(\frac{8kT_e}{\pi m_e}\right)^{1/2} \frac{E_H}{E_j} \exp\left(\frac{E_j}{kT_e}\right) \bar{g} , \tag{25}$$

where the value of $\bar{g}$ for argon was obtained experimentally as $\bar{g}=0.064$. We used this rate coefficient for the ionizations from all levels, although the application for the ionization from higher excited-levels seems to cause overestimation. However,

the excitation rates are much more rapid than the ionization rates, so that the population in the excited levels is under almost no influence of the ionization rates. The photo-ionization cross-sections of argon are discussed in the next section.

The $3d$-$5s$ transition is optically forbidden. The Bethe approximation gives the excitation cross-section for the optically forbidden transition as.

$$Q_{ij}(E) = \pi a_0^2 \frac{E_H}{E} B_{ij} . \tag{26}$$

(See Moiseiwitsch & Smith[19].)

The rate coefficient, by assuming the Maxwellian distribution for electron gas, reduces to

$$S_{ij}(T_e) = \pi a_0^2 B_{ij} \left(\frac{8kT_e}{\pi m_e}\right)^{1/2} \frac{E_H}{kT_e} \exp\left(-\frac{E_{ij}}{kT_e}\right) \tag{27}$$

The effective principal quantum numbers of the $5s$ and the $3d$ states are 2.894 and 2.851, respectively. We estimate the cross-section of the $3d$-$5s$ excitation using the $3p$- and the $3d$-state wavefunctions of a hydrogen atom, and obtain

$$B_{ij} = 6.4 \tag{28}$$

In Appendix *A*, the detailed explanations are described.

4.2 Atom-Atom Inelastic Collisions

There are no rigorous formulas for an estimation of ionization and excitation cross-sections due to atom-atom inelastic collisions. Hollenbach & Salpeter[9] proposed semi-empirical formulas with adjustable parameters for atom-atom ionization and excitation rates. Drawin[20], applying Thomson's ionization cross section of electron-atom collisions, obtained a simple formula. He showed that the formula is in good agreement with the quantum mechanical calculations and also with the experimental results. The cross-section given by Drawin is

$$Q_{jI}(E) = 4\pi a_0^2 \left(\frac{E_H}{E_j}\right)^2 \frac{m_a}{m_H} \xi_j \frac{2m_e}{m_a+m_e} h\left(\frac{E}{E_j}\right) \tag{29}$$

$$h(x) = \frac{x-1}{\left\{1+\frac{2m_e}{m_a+m_e}(x-1)\right\}^2} \tag{30}$$

where ξ_j is the number of equivalent electrons, and for argon, $\xi_1=6$ and $\xi_j=1$ $(j>1)$. By assuming the Maxwellian velocity distribution for colliding particles, the ionization rate coefficient can be written as

$$K_{jI} = \int_{v_j}^{\infty} Q_{jI}\left(\frac{m_a}{4} v_a^2\right) v_a f(v_a)\, dv_a , \quad v_j = \left(\frac{4E_j}{m_a}\right)^{1/2} \tag{31}$$

$$f(v_a) = 4\pi \left(\frac{m_a}{4\pi kT}\right)^{3/2} v_a^2 \exp\left(-\frac{m_a v_a^2}{4kT}\right), \tag{32}$$

where v_a is the relative speed of atoms. Accordingly,

$$K_{jI}(T) = 32\pi a_0^2 \left(\frac{E_H}{E_j}\right)^2 \left(\frac{kT}{\pi m_a}\right)^{1/2} \xi_j \frac{m_e m_a}{m_H(m_a+m_e)} \psi\left(\frac{E_j}{kT}\right), \tag{33}$$

where

$$\psi(x) = \int_x^\infty h(yx) y \exp(-y)\, dy . \tag{34}$$

Drawin gave an approximate formula

$$\psi(x) = \frac{1+2/x}{\left\{1+\frac{2m_e}{(m_e+m_a)x}\right\}^2} \exp(-x) . \tag{35}$$

In analogy to the ionization cross-section, Drawin & Emard[21] proposed the excitation cross-section:

$$Q_{ij}(E) = 4\pi a_0^2 \left(\frac{E_H}{E_{ij}}\right)^2 \frac{m_a}{m_H} \xi_j f_{ij} \frac{2m_e}{m_a+m_e} h\left(\frac{E}{E_{ij}}\right). \tag{36}$$

The excitation rate coefficient reduces similarly to

$$K_{ij}(T) = 32\pi a_0^2 \left(\frac{E_H}{E_{ij}}\right)^2 \left(\frac{kT}{\pi m_a}\right)^{1/2} \xi_i \frac{m_a m_e}{m_H(m_a+m_e)} \psi\left(\frac{E_{ij}}{kT}\right). \tag{37}$$

It should be mentioned that the rate coefficients of the transitions from the ground state must be divided by two in order to avoid counting like-like collisions twice.

5. Radiative Transition Rates

5.1 Bound-Bound Transition Probabilities

The transition probabilities between the coalesced levels are listed in Table 2. The transition probabilities between the actual levels are determined from the weighted mean of A-coefficients given in the NBS table[22] where possible. Otherwise, they are calculated by use of the Bates & Damgaard method[23]. The average probabilities of transition between a hydrogenic level and an actual level are obtained using the relation of

$$g_j A_{ji} = \sum_{l_j} g_{(n_j,l_j)} A_{(n_j,l_j),i} , \tag{38}$$

where n and l are respectively the principal and the angular quantum numbers of the hydrogenic grouped jth level. For transitions between hydrogenic levels, the approximate formula of a hydrogen atom is used:

$$A_{nm} = \frac{1.6\times10^{10}}{n^3 m(n^2-m^2)}\, s^{-1} . \tag{39}$$

5.2 Escape Factors of Line Radiations

The radiation-escape factor β_{ij} of line radiation for an i to j transition is defined by

$$(1-\beta_{ij})n_i A_{ij} = \left(n_j - \frac{g_j}{g_i} n_i\right) B_{ji} \int L(\nu) \int_0^{4\pi} I_\nu d\Omega d\nu , \tag{40}$$

(See Mitchner & Kruger[16]).

where $L(\nu)$, the line-shape factor, satisfies the normalization condition:

$$\int L(\nu) d\nu = 1 . \tag{41}$$

The radiation intensity $I_\nu(\Omega)$ is governed by the radiation transfer equation

$$\frac{dI_\nu}{ds} = \varepsilon - kI_\nu . \tag{42}$$

(See Griem[24].)

Here, the emission coefficient is written as

$$\varepsilon(\nu) = \frac{h\nu}{4\pi} n_i A_{ij} L(\nu) , \tag{43}$$

and the effective absorption coefficient, including the induced emission, is

$$k(\nu) = n_j \sigma_{ji}(\nu) - n_i \sigma_{ij}(\nu) . \tag{44}$$

As the absorption cross-section is expressed as

$$\begin{aligned} \sigma_{ji}(\nu) &= h\nu_{ij} B_{ji} L(\nu) , \\ &= \frac{\pi e^2}{m_e c} f_{ji} L(\nu) , \end{aligned} \tag{45}$$

the effective absorption coefficient is written in the form

$$k(\nu) = \frac{\pi e^2}{m_e c} n_j f_{ji} \left(1 - \frac{n_i}{n_j}\frac{g_j}{g_i}\right) L(\nu) . \tag{46}$$

The radiation transfer equation (42) can be integrated to yield

$$\begin{aligned} I_\nu(\Omega, s) = &\int_{s_0}^{s} \varepsilon(s') \exp\left[-\int_{s'}^{s} k(s'')ds''\right] ds' \\ &+ I(\Omega, s_0) \exp\left[-\int_{s_0}^{s} k(s')ds\right] \end{aligned} \tag{47}$$

The evaluation of this equation is mathematically difficult because of its isotropic

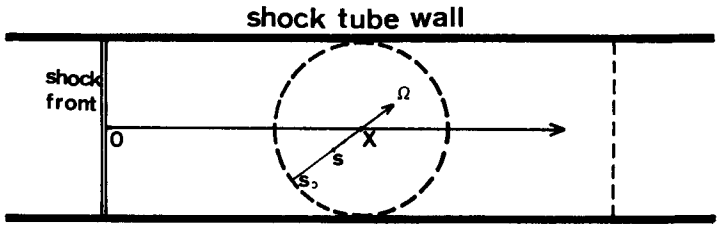

Fig. 2. Schematic diagram of shock tube flow and spherical model.

character. Horn[24] estimated the radiative cooling rate by assuming that the luminous gas near the point in question is at the same temperature and density for several types of geometrical domain. In this study, we employ his spherical volume model as shown in Figure 2. Then, the radiation intensity reduces to

$$I_\nu = \frac{2h\nu^3}{c^2} \frac{n_i g_j}{n_j g_i} \frac{1-\exp\left[-k(\nu)r_0\right]}{1-\dfrac{n_i}{n_j}\dfrac{g_j}{g_i}} \tag{48}$$

where r_0 is the radius of the sphere. Putting Equation (48) into (40), the escape factor reduces to

$$\beta_{ij} = \int L(\nu) \exp\left[-k(\nu)r_0\right] d\nu \tag{49}$$

The frequency dependence of the line absorption coefficients, in dense plasma, is determined mainly by the Doppler broadening and by the Stark broadening. The line-shape factor for the Stark broadening is described approximately by a Lorenzian profiel:

$$L(\nu) = \frac{1}{\pi} \frac{\Gamma_{ij}/4\pi}{(\nu-\nu_{ij})^2+(\Gamma_{ij}/4\pi)^2} . \tag{50}$$

Here, $\Gamma_{ij}/4\pi$ is the half width of the Stark broadening. The escape factor due to the Stark broadening is written as

$$\beta_{ij} = \frac{1}{\pi}\int_{-\infty}^{+\infty} \frac{\exp\left[-l/(1+u^2)\right]}{1+u^2}\, du , \tag{51}$$

with

$$u = \frac{\nu-\nu_{ij}}{\Gamma_{ij}/4\pi} , \tag{52}$$

where l is the optical depth such as

$$l = \frac{e^2 n_j f_{ji}}{m_e c(\Gamma_{ij}/4\pi)} \left(1-\frac{n_i}{n_j}\frac{g_j}{g_i}\right) r_0 , \tag{53}$$

The integral of (51) can be expressed in terms of the modified Bessel function of

the first kind:

$$\beta_{ij} = \exp\left(-\frac{l}{2}\right) I_0\left(\frac{l}{2}\right). \tag{54}$$

For the Doppler broadening, the line-shape factor is given by

$$L(\nu) = \frac{1}{\sqrt{\pi}} \frac{1}{\Delta\nu_d} \exp\left[-\left(\frac{\nu-\nu_{ij}}{\Delta\nu_d}\right)^2\right] \tag{55}$$

with the Doppler width

$$\Delta\nu_d = \frac{\nu_{ij}}{c}\sqrt{\frac{2kT}{m_a}}. \tag{56}$$

Transforming to a new variable

$$u = \frac{\nu-\nu_{ij}}{\Delta\nu_d} \tag{57}$$

the escape factor due to the Doppler broadening is written as

$$\beta_{ij} = \int \phi \exp\,(-g\phi) du \tag{58}$$

where ϕ, the normalization for $L(\nu)$, is

$$\phi(u) = \frac{1}{\sqrt{\pi}} \exp\,(-u^2) \tag{59}$$

and g, the optical depth, is

$$g = \frac{\pi e^2 n_j f_{ji}}{m_e c \Delta\nu_d}\left(1 - \frac{n_i}{n_j}\frac{g_j}{g_i}\right) r_0. \tag{60}$$

In order to obtain the relation between the escape factor and the optical depth, we make use of the approximate method of Hansen & McKenzie[26] who derived the approximate formula for the equivalent width of a spectral line. As the Gaussian profile has properties somewhat like a rectangular step function, they assumed

$$\phi(u) = \begin{cases} \dfrac{1}{2b} & |u| < b, \\ 0 & |u| > b, \end{cases} \tag{61}$$

where

$$b^2 = ln\left(e^{\pi/4} + \frac{g}{\sqrt{\pi}}\right). \tag{62}$$

The escape factor given by Equation (58), with use of the approximate profile (61), reduces to

$$\beta_{ij} = \exp\,(-g/2b)\,. \tag{63}$$

We compare the results of the numerical integrating of Equation (58) with the

values given by Equation (63), and obtain a fairly good agreement.

When the Stark and the Doppler broadening mechanisms act simulteneously, the line-shape factor is given by

$$\phi(u) = \frac{a}{\pi^{3/2}} \int \frac{\exp(y^2)}{a^2+(u-y)^2}\, dy\,, \tag{64}$$

where

$$u = \frac{\nu-\nu_{ij}}{\Delta\nu_d}\,,\quad a = \frac{\Gamma_{ij}/4\pi}{\Delta\nu_d}\,. \tag{65}$$

For the Voight profile, Hansen & MacKenzie[26] took

$$\phi(u) = \begin{cases} \dfrac{1}{2b} - \dfrac{a}{\pi b^2}\,, & |u| < b\,, \quad a < \dfrac{\pi}{4}\,, \\ \dfrac{a}{\pi u^2}\,, & |u| > b\,, \quad a < \dfrac{\pi}{4}\,, \\ \dfrac{\pi}{16a}\,, & |u| < \dfrac{4a}{\pi}\,, \quad a > \dfrac{\pi}{4}\,, \\ \dfrac{a}{\pi b^2}\,, & |u| > \dfrac{4a}{\pi}\,, \quad a > \dfrac{\pi}{4}\,. \end{cases} \tag{66}$$

With these approximate profiles, the escape factor given by Equation (58) becomes

$$\beta_{ij} = \begin{cases} \left(1-\dfrac{2a}{\pi b}\right)\exp\left[-g\left(\dfrac{1}{2b}-\dfrac{a}{\pi b^2}\right)\right] + \sqrt{\dfrac{a}{g}}\,\mathrm{erf}\left(\dfrac{1}{b}\sqrt{\dfrac{ga}{\pi}}\right), & a < \dfrac{\pi}{4}\,, \\ \dfrac{1}{2}\exp\left(-\dfrac{\pi b}{16a}\right) + \sqrt{\dfrac{a}{g}}\,\mathrm{erf}\left(\dfrac{1}{4}\sqrt{\dfrac{\pi g}{a}}\right), & a > \dfrac{\pi}{4}\,. \end{cases} \tag{67}$$

In the present calculations, the escape factors for the bound-bound transitions between the actual levels are determined from the above-mentioned formulas. The other line-radiation escape-factors are assumed to be $\beta_{ij}=1$.

5.3 Stark Broadenings

In dense plasmas, line shapes are influenced by interactions of the radiating atoms with the surrounding charged particles. This type of broadening, which is called the Stark broadening, has been investigated in the recent decade. The theory of the Stark broadening was reviewed by Baranger[27] and Griem[28]. Griem calculated the Stark broadening parameters for many neutral atom lines and listed them in tabulated form, in which the Stark widths of neutral argon are listed for 49 lines of transitions to $3p$, $3d$, $4s$ and $4p$ states. In the present model, the energy levels are gathered according to common configurations, so that the lines are also coalesced, as shown in Table 2. As the Stark profiles of lines in each multiplet are expected to have approximately the same width, within a

certain precision, we choose an appropriate value as a coalesced line among the Stark-width data of the corresponding lines given by Griem. For other lines which are not found in the tabulated form, we estimate them by calculating electron-impact broadening-widths by use of the adiabatic impact approximation

$$\frac{\Gamma_{ij}}{2} = \left(\frac{\pi}{2}\right)^{5/3} \frac{\Gamma(\frac{1}{3})}{3^{2/3}} \left(\frac{h}{2\pi m_e}\right)^{4/3} n_e \sum_j |\langle i|r|j\rangle|^2 (v^{1/3}) , \tag{68}$$

$$(v^{1/3}) = \int_0^\infty v^{1/3} f(v) dv ,$$

$$= \frac{4}{9} (6\pi)^{1/2} 2^{2/3} \left(\frac{kT_e}{m_e}\right)^{1/6} \frac{1}{\Gamma(\frac{1}{3})} , \tag{69}$$

(See Griem, Baranger, Kolb and Oertel[29].)

where $\langle i|r|j\rangle$ is the matrix element which, in this study, is determined from the Coulomb approximation.

In Table 2, the (half) half widths of the Stark broadening used in the present investigation are listed at the electron density of 10^{16} cm^{-3} and the several electron temperatures. For other electron densityies n_e, they are converted by multiplying by $(n_e/10^{16}\text{cm}^{-3})$.

5.4 Free-Bound Transition Rate

The radiative capture cross-section into the *jth* level of a free electron (σ_{cj}) is related with the the photo-ionization cross-section (σ_j)

$$\sigma_{cj}(v) = \frac{g_j}{Z_I} \left(\frac{h\nu}{m_e v c}\right) \sigma_j(\nu) , \tag{70}$$

(See Zel'dovich & Raized[30].)

where the energy of a photon emitted during the radiative capture is

$$h\nu = \frac{1}{2} m_e v^2 + E_j . \tag{71}$$

The rate of the photo-recombination is written as

$$A_{Ij} n_e^2 = n_e^2 \int_0^\infty \sigma_{cj}(v) v f(v) dv , \tag{72}$$

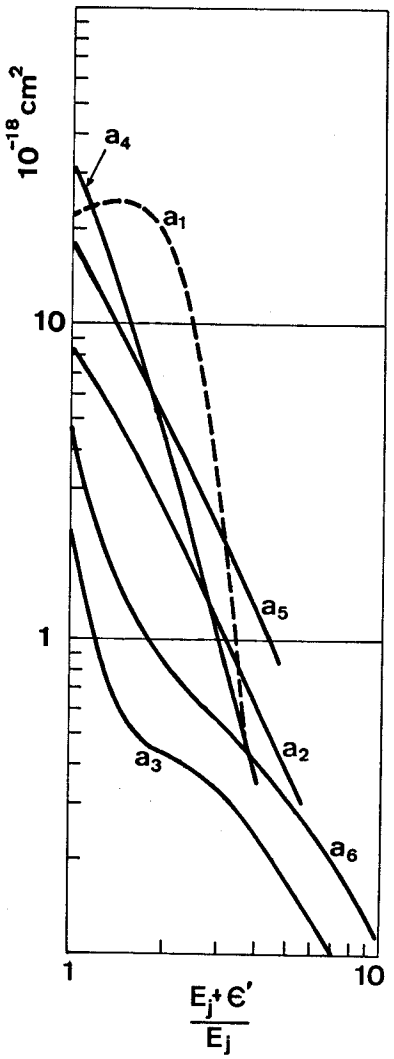

Fig. 3. Photo-ionization cross-sections for actual levels (ground ($3p$), $4s$, $4p$, $3d$, $5s$, $5p$ levels).

where $f(v)$ is the velocity distribution of electron gas.

In Figure 3, the photo-ionization cross-sections of actual levels are shown. The cross-section of the ground state was calculated by Kennedy & Manson[31]. For five actual excited-states, the cross-sections are determined from the formula of Burgess & Seaton[32]. For hydrogenic states, Kramer's formula can be used:

$$\sigma_n(\nu) = \frac{64}{3\sqrt{3}} \alpha \pi a_0^2 n \left(\frac{E_n}{h\nu}\right)^3 , \tag{73}$$

where n is the principal quantum number. In order to derive A_{Ij}, we assume the photo-ionization cross-section in the form

$$\sigma_j(\nu) = a_j(0) \left(\frac{E_j}{h\nu}\right)^m \tag{74}$$

where $m=2$ is used for $j=2$, 3, 5 and 6, and $m=3$ is used for $j=4$ and $j \geq 7$. Substituting the Maxwellian distribution function for $f(v)$, the coefficient is represented by

$$A_{Ij} = \begin{cases} \dfrac{g_j}{2Z_I} \left(\dfrac{8kT_e}{\pi m_e}\right)^{1/2} \dfrac{\alpha^2 a_j(0)}{2} \dfrac{E_j}{E_H} \left(\dfrac{E_j}{kT_e}\right)^2 \exp\left(\dfrac{E_j}{kT_e}\right) E_i\left(-\dfrac{E_j}{kT_e}\right), & \text{for } m = 3 , \\ \dfrac{g_j}{2Z_I} \left(\dfrac{8kT_e}{\pi m_e}\right)^{1/2} \dfrac{\alpha^2 a_j(0)}{2} \dfrac{E_j}{E_H} \dfrac{E_j}{kT_e}, & \text{for } m = 2 , \end{cases} \tag{75}$$

where E_i is the exponential integral function:

$$E_i(-x) = \int_x^\infty \frac{e^{-x}}{x} dx . \tag{76}$$

The emission coefficient for radiative capture to the *jth* level can be written as

$$\varepsilon_j = n_e^2 \int \frac{h\nu}{4\pi} \sigma_{cj}(v) f(v) v dv . \tag{77}$$

It also reduces to

$$\varepsilon_j = \begin{cases} \dfrac{n_e^2}{4\pi} \dfrac{g_j}{2Z_I} \left(\dfrac{8kT_e}{\pi m_e}\right)^{1/2} \dfrac{\alpha^2 a_j(0)}{2} \dfrac{E_j}{kT_e} \dfrac{E_j}{E_H} E_j , & \text{for } m = 3 , \\ \dfrac{n_e^2}{4\pi} \dfrac{g_j}{2Z_I} \left(\dfrac{8kT_e}{\pi m_e}\right)^{1/2} \dfrac{\alpha^2 a_j(0)}{2} \dfrac{E_j}{kT_e} \dfrac{E_j}{E_H} , & \text{for } m = 2 . \end{cases} \tag{78}$$

The escape factors for radiative recombination are defined by

$$(1-\beta_{Ij}) n_e^2 A_{Ij} = n_j \int \frac{I_\nu(\Omega)}{h\nu} \sigma_j'(\nu) d\nu d\Omega , \tag{79}$$

$$\sigma_j' = \sigma_j \left(1 - \frac{n_j^*}{n_j} e^{-h\nu/kT_e}\right) , \tag{80}$$

where

$$n_j^* = n_e^2 \frac{g_j}{2Z_I} \frac{h^3}{(2\pi m_e k T_e)^{3/2}} \exp\left(\frac{E_j}{kT_e}\right). \tag{81}$$

In the present study, we do not use this formula, but for sinplicity we assume

$$\beta_{Ij} = \begin{cases} 0, & \text{for } j = 1, \\ 1, & \text{for } j \geq 2. \end{cases} \tag{82}$$

6. Energy Transfer Rates

The energy loss rate due to atom-atom inelastic collisions is the sum of the rate for energy compensated only for excitation and ionization E_A, and the rate at which thermal energy is given to the free electrons ejected by atom-atom ionization ε_A. We write these terms as

$$E_A = n_a \sum_j \left[\sum_{i>j} (n_j K_{ji} - n_i K_{ij}) E_{ji} + (n_j K_{jI} - n_e^2 K_{Ij}) E_j\right] \tag{83}$$

$$\varepsilon_A = n_a \sum_j (n_j K_{jI} - n_e^2 K_{Ij}) \bar{\varepsilon}_j \tag{84}$$

Here, $\bar{\varepsilon}_j$ is the average kinetic energy of the electrons ejected from the *jth* level. Belozerov & Measures[33], by assuming an equi-partition of the energy among the atom, ion and electron resulting from atom-atom ionization collision, gave the formula.

$$\bar{\varepsilon}_j = \frac{2}{3} kT \frac{E_j + 3kT}{E_j + 2kT} \tag{85}$$

We use it in this study. However, the validity of their assumption of energy equi-partition is not so clear, and therefore requires further investigation.

The rate of energy loss of the free electrons due to atom-electron inelastic collisions is

$$E_I = n_e \sum_j \left[\sum_{i>j} (n_j S_{ji} - n_i S_{ij}) E_{ji} + (n_j S_{jI} - n_e^2 S_{Ij}) E_j\right] \tag{86}$$

The rate of energy loss of the electrons due to bremsstrahlung radiation is shown by Pomerantz[34] as follows

$$E_B = \frac{64\pi^{3/2} e^6}{3\sqrt{6}\, m_e^{3/2} k^{1/2} c^3} \frac{n_e^2}{T_e^{1/2}} \frac{kT_e}{h} g \tag{87}$$

In the present calculations, the Gaunt factor $g=1$ is used.

Owing to radiative recombination, electrons with some kinetic energy disappear in the electron gas. The rate of energy loss due to radiative recombination can be written as

$$E_c = \sum_j (4\pi\varepsilon_j - n_e^2 A_{1j} E_j) \tag{88}$$

The rate of energy transferred to the electrons by the heavy particles during elastic collisions is given by

$$E_T = n_e \left(\frac{m_e}{m_a}\right) 3k(T - T_e)\ (\nu_{ea} + \nu_{ei}) \tag{89}$$

The collision frequencies of electron-atom and electron-ion elastic collisions are respectively given by

$$\nu_{ea} = n_a \left(\frac{8kT_e}{\pi m_e}\right)^{1/2} Q_{ea} \tag{90}$$

$$\nu_{ei} = n_i \left(\frac{8kT_e}{\pi m_e}\right)^{1/2} Q_{ei} \tag{91}$$

The elastic cross-section of argon atoms with electrons, given by Devoto[35], is approximately represented by[36]

$$Q_{ea} = \begin{cases} (0.713 - 4.5\times10^{-4} T_e + 1.5\times10^{-7} T_e^2)\times10^{-16}\,\mathrm{cm}^2 \\ \qquad\qquad \text{for } T_e < 3000^\circ K \\ (-0.488 + 3.96\times10^{-4} T_e)\times10^{-16}\,\mathrm{cm}^2 \\ \qquad\qquad \text{for } T_e > 3000^\circ K \end{cases} \tag{92}$$

The cross-section between electrons and ions is given by

$$Q_{ei} = \frac{2\pi e^4}{9(kT_e)^2} ln\left(\frac{9k^3 T_e^3}{4\pi e^6 n_e}\right) \tag{93}$$

7. Results and discussions

Calculations are performed for behaviors of flow properties and excited-level population-densities in the ionization relaxation region behind a strong shock moving into stationary argon gas. The numerical computations are carried out in the following manner. A computer program for the collisional and radiative model was developed to calculate Equation (8) for the excited-level population-densities, $n_j (j \geq 2)$, with the input of ρ, n_e, n_1, T and T_e. Another program for the gasdynamics calculation was made to numerically integrate Equations (3), (4), (5) and (7) with the relations of (1), (2) and (6) for the evaluation of n_e, n_1, T and T_e. In order to start computations, we assume that there are no electrons and no excited-atoms at the shock front: $n_e = 0$ and $n_j = 0$ $(j \geq 2)$ at $x = 0$. The other values are determined from the Rankine-Hugoniot relation. The computations, which have been performed on the FACOM M200 computer in the Kyoto University Data Processing Center, require less than 10 minutes to per-

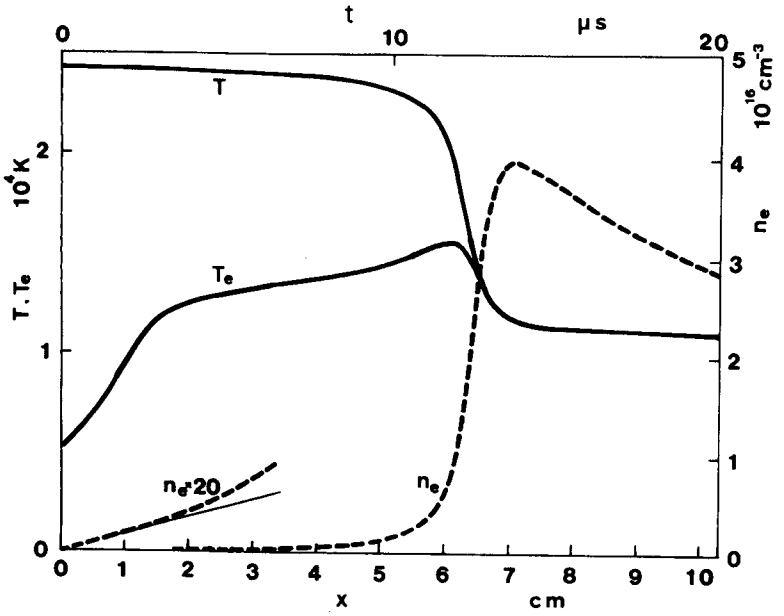

Fig. 4. Variations of temperatures of heavy particles (T), electron temperature (T_e) and electron density (n_e) as functions of distance from shock front (x) and laboratory time after shock arrival (t) for the condition of $Ms=16$, $p_1=1$ torr, $T_1=300$ K.

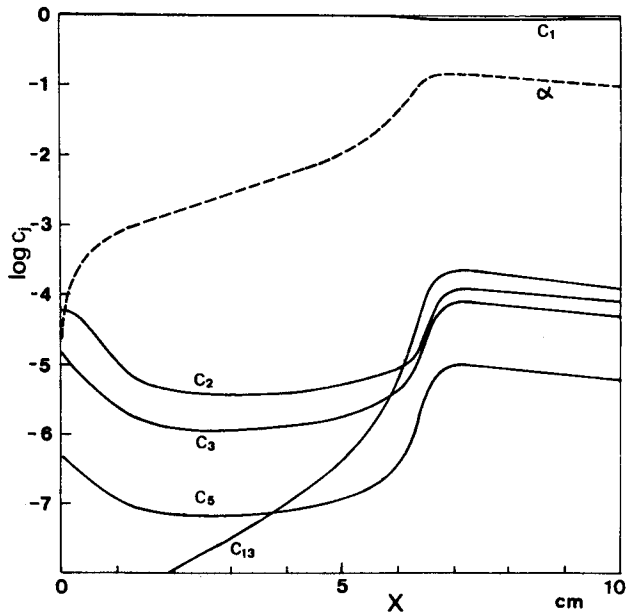

Fig. 5. Variations of concentrations of jth-level atoms (c_j) and degree of ionization (α). Subscripts $j=1, 2, 3, 5$ and 13 refer to ground($3p$), $4s$, $4p$, $5s$ and hydrogenic ($n=10$) levels respectively.

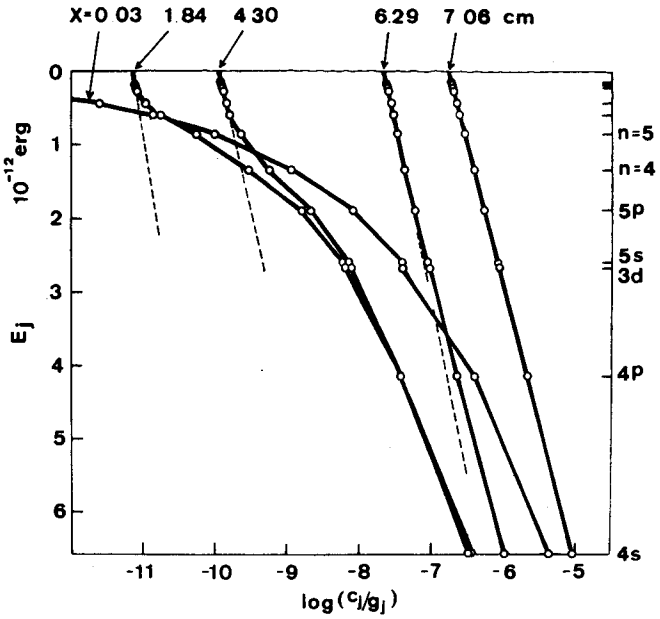

Fig. 6. Boltzmann plots for excited-level concentrations where x means location measured from shock front.

form.

The results of the computations are shown in Figures 4–8 for the following conditions:

$$U_s = 5.14 \text{ Km/s}, \quad M_s = 16 ,$$
$$p_1 = 1 \text{ torr}, \quad T_1 = 300 \text{ K}, \quad r_0 = 2 \text{ cm} .$$

Figure 4 shows the variations of the temperature of heavy particles, the electron temperature and the electron density as functions of the distance from the shock front. Figure 5 shows the variations of the concentrations of the *jth*-level atoms ($c_j = m_a n_j / \rho$). The Boltzmann plots for the excited-level poplation-distributions in the relaxation region are presented in Figure 6, where the dotted lines denote the distributions of the excited states in local thermodynamic equilibrium with free electrons. From these results, the ionization relaxation region can be observed to consist of the initial ionization, induction, rapid ionizing and equilibrium parts.

Striking features of the present results of the multi-step process model are the drop of the electron temperature and the peaks of the lower level populations in the initial ionization region, $0 \leq x \leq 1.5$ cm. The electron temperature is lowest immediately behind the shock front, and afterwards it recovers to a quasi-steady

value according to the decrease of the lower-level population-density. In the present model, the initial kinetic energy of electrons, produced by atom-atom collisional ionization, is transferred according to Equation (85), so that the ejected electrons have initial temperatures between $(4/9)T$ and $(2/3)T$, where T is the heavy temperature. Evidently, the electron temperature falls below these values in the initial ionization region. This drop of the electron temperature means that the kinetic energy of the electron gas is consumed by the inelastic collisions of the electrons. The excited-level population-distribution immediately behind the shock front, mainly determined by the atom-atom inelastic collisions, is severely overpopulated from the local equilibrium distribution, as shown by the Boltzmann plot at $x=0.03$ cm in Figure 6. Therefore, the inelastic collisions of the electrons with excited-atoms take place remarkably and the electron temperature drops severly. As the electron density increases gradually in the initial ionization region, the population-density in the lower level decreases. This is because the inelastic collsions of the electrons tend to turn the excited-level population-distribution towards the local equilibrium distribution. The electron temperature, determined mainly by balancing the energy gain due to the elastic collisions of electrons with heavy particles and the energy loss caused by the inelastic collisions of electrons with excited atoms, rises according to the reduction of the excess of the excited-level population-distribution from the local equilibrium distribution.

The concentrations of the lower levels are almost invariable, from $x=1.5$ to 5 cm, in spite of a gradual increasing in the concentrations of the higher levels and the degree of ionization. The population-distribution in the lower levels, which are in steady state and considerablly overpopulated from the local equilibrium values, is seen to be determined by balancing the atom-atom excitation rates and the rates of excitation due to the collisions between the excited-atoms and electrons. The detailed mechanism is not so clear and requires further investigation. Meanwhile, the population-distribution of the excited atoms approaches to the local equilibrium distribution from the upper levels.

When the excition due to the inelastic collisions of the ground-level atoms and electrons becomes dominant ($x \geq 7$ cm), the ionization proceeds rapidly and population-densities in the excited levels approach to their equilibrium values. After equilibration, the radiative cooling effect appears as a slight decay of the electron density. In this radiative cooling region, the Saha-Boltzmann distribution is established in the excited states.

The line radiation energy loss per unit volume per unit time can be expressed as

$$q_{ij} = n_i A_{ij} \beta_{ij} E_{ij} \tag{94}$$

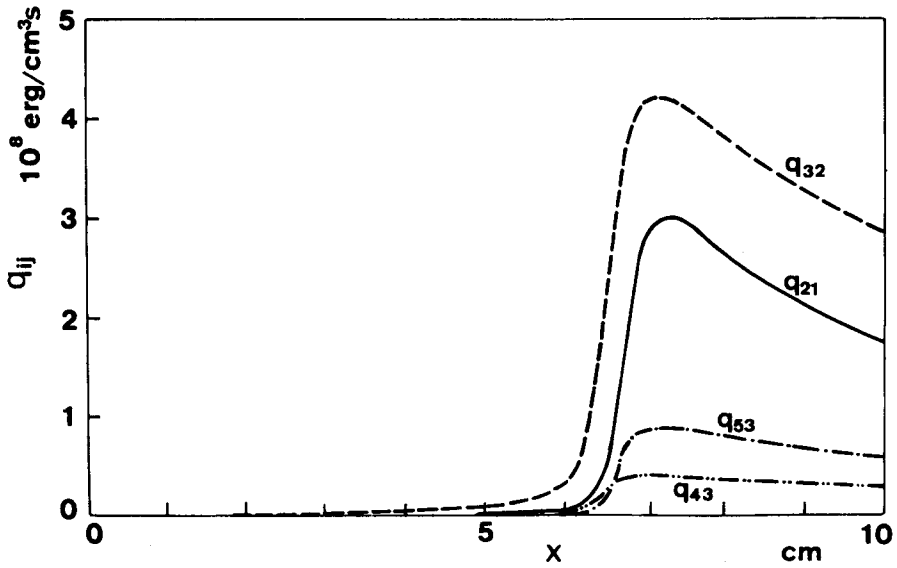

Fig. 7. Variations of line-radiation energy losses; q_{21}: $4s$-$3p$ transition, q_{21}: $4p$–$4s$, q_{43}: $3d$–$4p$, q_{53}: $5s$–$4p$.

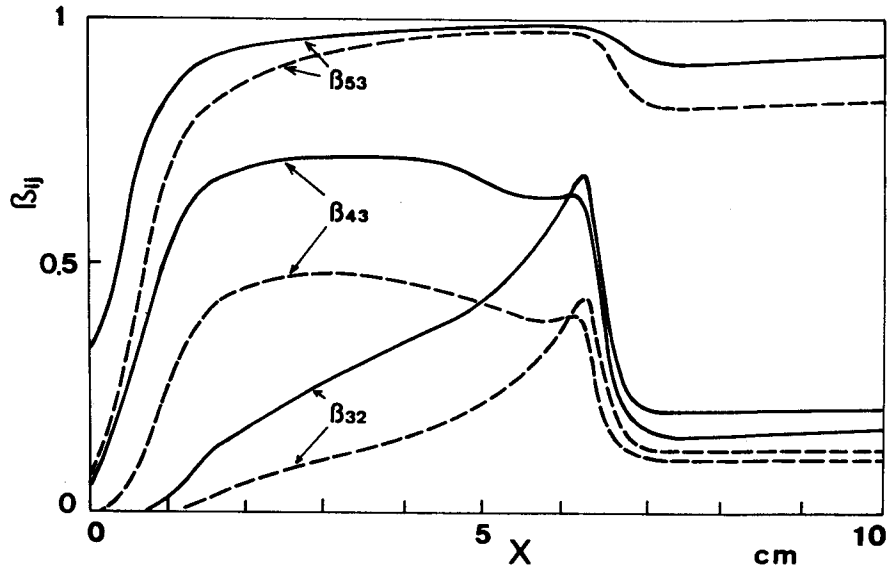

Fig. 8. Variations of radiation escape factors. Solid lines refer to shock tube radius $r_0=2$ cm, and dotted lines to $r_0=5$ cm.

where the subscripts i and j refer to the emitting and the absorbing levels, respectively, and β_{ij} is the radiation-escape factor defined in Equation (40). The variations of the radiative energy loss are shown in Figure 7 for several lines. Figure 8 shows the variations of the radiation-escape factors. For the resonance series,

the radiations are almost trapped owing to the self-absorption: $\beta_{j1} \simeq 0$. As discussed in Section 5, several broadening mechanisms contribute to the self-absorption in the lines. In the initial ionization region, where the electron density is low and the temperature of heavy particles is high, the Doppler broadening dominates the collisional and natural broadening. On the other hand, in the equilibrium region, where the electron density is over $10^{16}\,\mathrm{cm}^{-3}$, the Stark broadening mechanism plays an important role for the line broadening.

We find no peaks of radiative energy loss in any of the lines of Figure 7, although there are peaks in the concentrations of the emitting atoms in the initial ionization. Because the concentration of the absorbing level is more populated than that of the emitting level, the escape factor becomes very low when the concentration of the absorbing level becomes high, as shown in Figure 8. Consequently, the line radiations are trapped due to the self-absorption in the initial ionization region.

In the equilibrium region, the effects of radiative cooling, causing a reduction of the enthalpy of the ionized gas, appear as a decay of the electron density in the equilibrium region. The population-distribution in the excited states, which are determined by collisional mechanisms in the present conditions, is negligibly influenced by radiative transitions.

We calculate the specific line-intensity for spectropcopic measurements in shock-tube experiments as

$$I_{ij} = \int_0^\infty I_\nu d\nu \tag{95}$$

where

$$I_\nu = \frac{2h\nu^3}{c^2} \frac{n_i g_j}{n_j g_i} \frac{1-\exp\{-k(\nu)d\}}{1-\dfrac{n_i}{n_j}\dfrac{g_j}{g_i}} \tag{96}$$

and $d=2\,r_0$, the shock tube diameter. The detailed descriptions of the line intensity are written in Appendix *B*.

Figure 9 shows the variations of the line-radiation intensity. There are no peaks of the line-radiation intensities which correspond to the peaks of the population-densities of the excited atoms in the initial ionization region because of the self-absorption.

Kamimoto, Teshima & Nishimura[10] investigated the behavior of excited-level population-densities in the ionization relaxation region of shock-heated argon, considering the 4-step model. It is seen in their theoretical results that the population-densities of the lower excited-states have peaks, and the electron temperature has a drop in the initial ionization zone. In their experimental results of

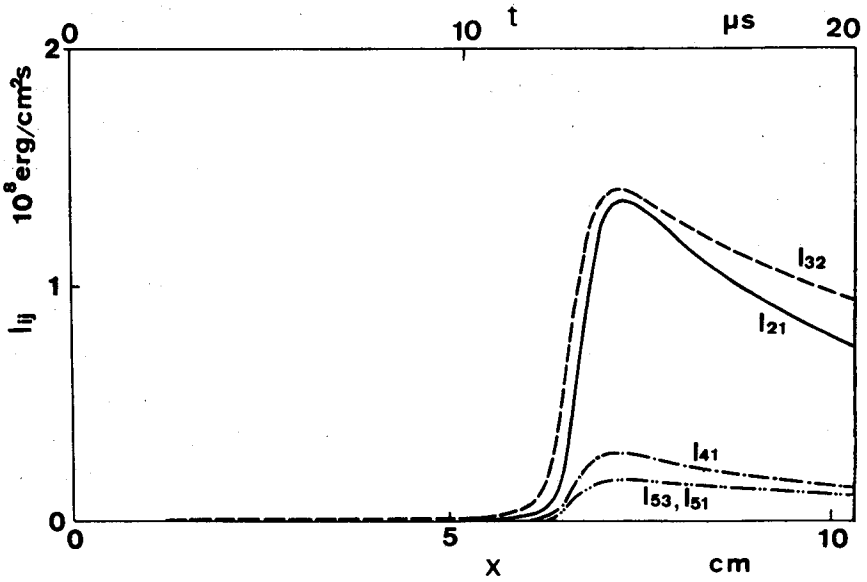

Fig. 9. Variations of line intensities.

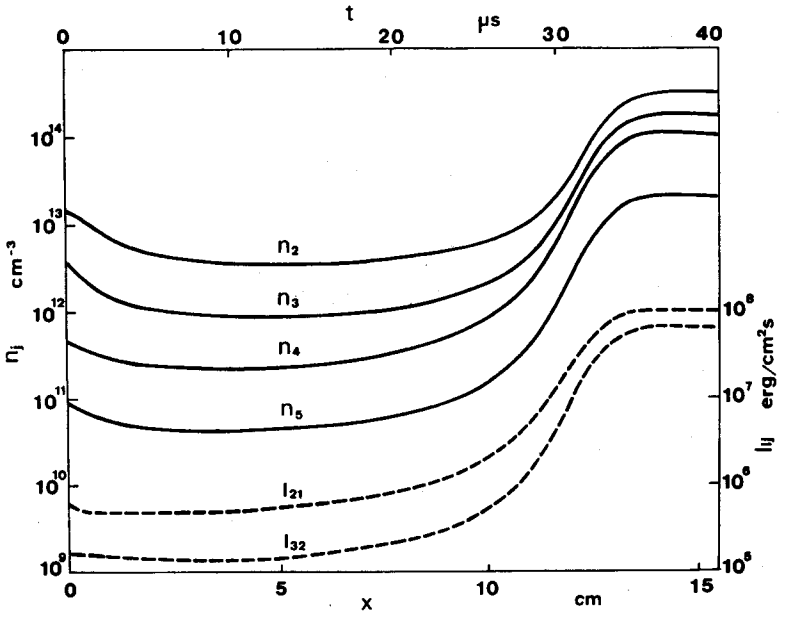

Fig. 10. Variations of population densities and line intensities behind moving shock at $Ms=12$, $p_1=5$ torr, $T_1=300$ K Subscripts $j=1, 2, 3$ refer to ground ($3p$), $4s$, $4p$ states, respectively x is distance from shock front, and t is time after shock arrival.

spectroscopic measurements, made in a shock tube with a diameter of 10 cm, no peaks of line-intensities for $5p$-$4s$ and $4s$-$3d$ transitions are observed immediately behind the moving shock at $M_s=15.7$ and $p_1=1$ torr. The present simulations for the behaviors of the excited-level population-densities and the line-intensities agree qualitatively with their theoretical and experimental results.

Figure 10 shows the results of computations for the following conditions

$$U_s = 3.87\ Km/s,\quad M_s=12\,,$$
$$p_1 = 5\ torr,\quad T_1 = 300\ K,\quad r_0 = 2\ cm\,.$$

In this case, we observe peaks of the lower-level populationdensities in the initial ionization region. The densities of the $4s$ and $4p$ states are over twice as much immediately behind the shock front as in the recession region from 1 to 5 cm. The line intensities are almost invariable from the initial region through the recession region.

Wojciechowski & Weymann[11] made a spectroscopic investigation of the initial ionization region behind a moving shock in argon in a shock tube with a diameter of 3.8 cm. It was observed in the oscilloscope traces for the line-intensities of $5s$-$4p$ and $4p$-$4s$ transitions at $M_s=10.6$ and $p_1=5$ *torr* that in a small inception time a steady-state intensity exsists which slowly steepens into an off-scale inten-

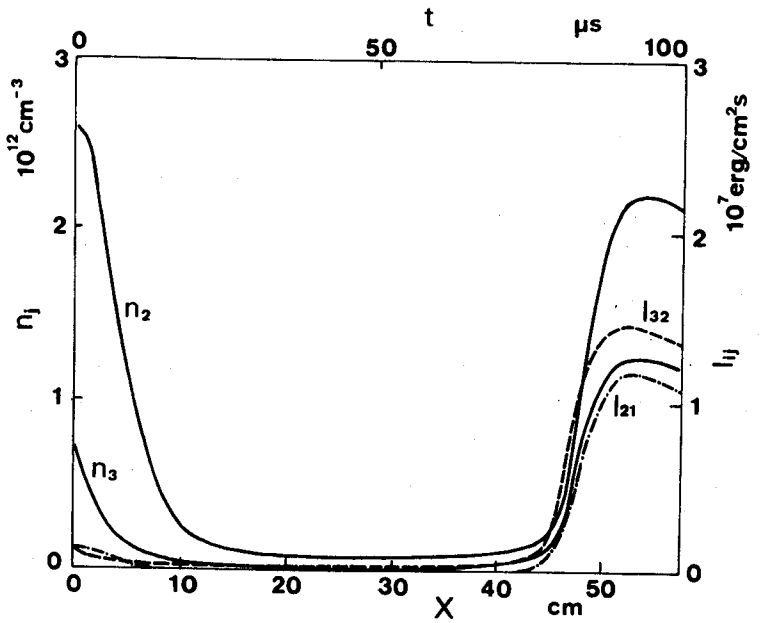

Fig. 11. Variations of population densities and line intensities behind moving shock at $Ms=18$, $p=0.1$ torr, $T_1=300$ K.

sity. Coates & Gaydon[37] measured the line-emission intensities from shock-heated argon to determine transition probabilities of argon. The record of intensity at 6965 A of $4p$-$4s$ transition at $M_s=11.3$ and $p_1=5.53$ torr, shown in their paper, agrees qualitatively with the variation of the line intensity I_{32} in Figure 10.

Lastly, we consider the case for the following conditions:

$$U_s = 5.81\ Km/s,\quad M_s = 18\,,$$
$$p_1 = 0.1\ torr,\quad T_1 = 300\ K,\quad r_0 = 2\ cm\,.$$

In this case, the profile of the ionization relaxation is more drastic because the shock is stronger. Also, the optical depth is thinner because the initial density is lower, compared with previous cases. Figure 11 shows the variations of densities of the first and second excited-level atoms and the intensities of the corresponding lines. The density of the first excited-state is highest immediately behind the shock front, and the excited-level population-densities have sharp initial peaks. In this case, small peaks of line-intensities are seen in the initial ionization region.

8. Conclusions

A rigorous formulation has been made for the description of excited-level population-densities and gasdynamic properties in nonequilibrium ionizing argon gas. In the formulation, the structure of an argon atom is assumed to consist of six actual levels and higher hydrogenic levels. We have considered the contributions of atom-atom inelastic collisions as well as atom-electron inelastic collisions for excitation and ionization. For radiative transitions, the effects of self-absorption in lines have been estimated.

Applying the collisional and radiative model for argon plasma, we have calculated the ionization relaxation phenomena behind moving shocks in argon. The ionization relaxation regions have been shown to consist of the initial ionization, induction, rapid ionizing and equilibrium parts. Immediately behind a shock front, the population-distribution in the lower levels, mainly determined from the atom-atom collisional process, is severely overpopulated relative to the local equilibrium distribution. In the initial ionization region, the population-densities in the lower levels decrease because the inelastic collisions of electrons tend to reduce the excess of the population-distribution from the local equilibrium distribution. In the following induction region, the densities in the lower levels, seemingly determined by balancing the excitation rates due to atom-atom collisions with those due to electron-excited-atom collisions, are in steady state in spite of a gradual increase of the population densities in the upper levels. In the profiles of the excited-level population-density, sharp peaks of lower level populations

appear in the initial ionization region because the populations are more numerous immediately behind the shock front than in the induction region.

Simulations of line-intensity have been carried out for spectroscopic measurements in shock tubes. The results show that it is difficult to observe peaks of line-intensities due to self-absorption in the lines. This is because the populations of the absorbing levels are more severely overpopulated than those of the emitting levels.

Appendix A Estimation of the 3*d*-5*s* excitational cross-section of argon

The Bethe approximation gives the excitational cross-section for the optically-forbidden transition as

$$Q_{ij} = \pi a_0^2 \frac{E_H}{E} |(z^2)_{ij}|^2 , \tag{A1}$$

$$(z^2)_{ij} = \frac{1}{a_0^2}\int \varphi_i z^2 \varphi_j d\boldsymbol{r} , \tag{A2}$$

(See Moiseiwitsch & Smith[19].)

where φ_i and φ_j are wave functions of the atoms in the initial and final states, respectively. For a one-electron wave function such as

$$\varphi_{nlm} = R_{nl}(r) Y_{lm}(\theta, \phi) , \tag{A3}$$

the term (A2) can be written as

$$(z^2)_{ij} = (r^2)_{ij}(\mu^2)_{ij} , \tag{A4}$$

with

$$(r^2)_{ij} = \int R_{n_j l_j}(r) r^2 R_{n_i l_i}(r) r^2 dr , \tag{A5}$$

and

$$(\mu^2)_{ij} = \int Y^*_{l_j m_j}(\theta, \phi) \cos^2\theta Y_{l_i m_i}(\theta, \phi) d\cos\theta d\phi . \tag{A6}$$

Averaged over the initial substates, and summed over the final substates, $(\mu^2)_{ij}$ reduces to

$$(\mu^2)^2_{ij} = \begin{cases} \dfrac{2}{15}\dfrac{l_i(l_i-1)}{(2l_i-1)(2l_i+1)}, & l_j = l_i-2 \\ \dfrac{1}{15}\dfrac{8l_i^2+8l_i-5}{(2l_i-1)(2l_i+3)}, & l_j = l_i \\ \dfrac{2}{15}\dfrac{(l_i+1)(l_i+2)}{(2l_i+1)(2l_i+3)}, & l_j = l_i+2 . \end{cases} \tag{A7}$$

(See Carson[37].)

For the $3d$-$5s$ transition, putting $l_i=2$ and $l_j=0$, we have

$$(\mu^2)^2_{3d,5s} = \left(\frac{2}{15}\right)^2 . \tag{A8}$$

We estimate the term (A5) of the $3d$-$5s$ transition using the $3s$- and $3d$-state wave functions of a hydrogen atom because the effective quantum numbers of the $5s$- and $3d$-states are 2.894 and 2.851, respectively. Putting

$$R_{30}(r) = \frac{1}{9\sqrt{3}}\left\{6-6\left(\frac{2r}{3}\right)+\left(\frac{2r}{3}\right)^2\right\}e^{-r/3} , \tag{A9}$$

$$R_{32}(r) = \frac{1}{9\sqrt{30}}\left(\frac{2r}{3}\right)^2 e^{-r/3} , \tag{A10}$$

into (A6) and integrating

$$\int_0^\infty dr\, r^4 R_{30} R_{32} = \frac{1}{2^5\sqrt{10}}\int_0^\infty (6\rho^6-6\rho^7+\rho^8)e^{-\rho}d\rho , \tag{A11}$$

and we obtain

$$|r^2|_{ij} = 142.3 . \tag{A12}$$

Appendix B Line intensities for measurements outside of shock tubes.

We consider the line intensities for emission spectroscopy, measured by an observer outside of the shock tubes. The arrangement is shown in Figure B1. The specific intensities of radiation along a certain direction are written as

$$I_\nu(\Omega, s) = \int_{s_0}^{s} \varepsilon(s') \exp\left[-\int_{s'}^{s} k(s'')ds''\right]ds' + I(\Omega, s_0) \exp\left[-\int_{s_0}^{s} k(s')ds\right] . \tag{B1}$$

(See Equation (47).)

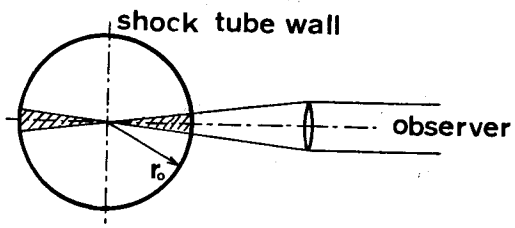

Fig. B1. Schematic diagram of cross section for shock tube and optical arrangement.

For simplicity, we assume a small solid angle and a homogeneous gas volume. Then, the radiation intensity per unit solid angle can be written as

$$I_\nu = \frac{2h\nu^3}{c^2}\frac{n_i g_j}{n_j g_i}\frac{1-\exp\left[-k(\nu)d\right]}{1-\dfrac{n_i g_j}{n_j g_i}} , \tag{B2}$$

where $d=2\cdot r_0$ is the diameter of the shock tube. It is integrated to obtain the total line intensity:

$$I_{ij}=\frac{n_i g_j}{n_j g_i}\frac{2h\nu_{ij}^3/c^2}{1-\frac{n_i g_j}{n_j g_i}}W, \tag{B3}$$

where the equivalent width of a spectral line is defined as

$$W=\int_0^\infty\{1-\exp[-k(\nu)d]d\nu\,. \tag{B4}$$

For the Doppler and the Voigt profiles, Hansen & McKenzie[26] proposed analytic approximations for the equivalent widths. They assumed a rectangular step function for the Gaussian profile:

$$\phi(u)=\begin{cases}\frac{1}{2b}, & |u|<b,\\ 0, & |u|>b,\end{cases} \tag{B5}$$

$$b^2=ln(e^{\pi/4}+g/\sqrt{\pi})\,, \tag{B6}$$

where g is the optical depth defined as

$$g=\frac{\pi e^2 n_j f_{ji}}{m_e c\Delta\nu_d}\left(1-\frac{n_i g_j}{n_j g_i}\right)d\,, \tag{B7}$$

with the Doppler width

$$\Delta\nu_d=\frac{\nu_{ij}}{c}\sqrt{\frac{2kT}{m_a}}\,, \tag{B8}$$

and obtained

$$\frac{W}{\Delta\nu_d}=2b\left\{1-\exp\left(-\frac{g}{2b}\right)\right\}. \tag{B9}$$

For the Voigt profile, they use such an approximate profile as

$$\phi(u)=\begin{cases}\frac{1}{2b}-\frac{a}{\pi b^2}, & |u|<b,\quad a<\frac{\pi}{4},\\ \frac{a}{\pi u^2}, & |u|>b,\quad a<\frac{\pi}{4},\\ \frac{\pi}{16a}, & |u|<\frac{4a}{\pi},\quad a>\frac{\pi}{4},\\ \frac{a}{\pi b^2}, & |u|>\frac{4a}{\pi},\quad a>\frac{\pi}{4},\end{cases} \tag{B10}$$

where

$$a = \frac{\Gamma_{ij}/4\pi}{\Delta\nu_d}. \tag{B11}$$

The equivalent width becomes

$$\frac{W}{\Delta\nu_d} = \begin{cases} 2b\left[\exp\left(-\frac{ga}{\pi b^2}\right) - \exp\left(\frac{ga}{\pi b^2} - \frac{g}{2b}\right)\right] + 2(ga)^{1/2} erf\left(\frac{ga}{\pi b^2}\right)^{1/2}, \\ 2(ga)^{1/2} erf\left(\frac{g\pi}{16a}\right), \end{cases} \tag{B12}$$

for the Voigt profiles.

As the Stark broadening has the Lorentz profile:

$$\phi(u) = \frac{1}{1+u^2}, \tag{B13}$$

its equivalent width reduces to

$$\frac{W}{\Gamma/4\pi} = \pi z \exp\left(-\frac{z}{2}\right)\left[I_0\left(\frac{z}{2}\right) + I_1\left(\frac{z}{2}\right)\right], \tag{B14}$$

where z is the optical depth:

$$z = \frac{e^2 n_j f_{ji}}{m_e c(\Gamma_{ij}/4\pi)}\left(1 - \frac{n_i g_j}{n_j g_i}\right) d, \tag{B15}$$

Here, I_0, I_1 are the modified Bessel functions of the first kind.

References

1) H. Petschek and S. Byron; Ann. Phys. **1** 270 (1957).
2) H.D. Weymann; Univ. Maryland, Institute for Fluid Mech. Tech. Note BN-144 (1958).
3) H. Wong and D. Bershader; J. Fluid Mech. **26** 459 (1966).
4) L.M. Biberman and I.T. Yakubov; Soviet Phys.-Tech. Phys. **8** 1001 (1964).
5) M.I. Hoffert and H. Lien; Phys. Fluids **10** 1769 (1967).
6) P.E. Oettinger and D. Bershader; AIAA J. **5** 1625 (1967).
7) D.L. Chubb; Phys. Fluids **11** 2363 (1968).
8) P.C.T. de Boer and P.R. Grimwood; Bull. Am. Phys. Soc. **13** 808 (1968).
9) D.J. Hollenbach and E.E. Salpeter; J. Chem. Phys. **50** 4157 (1969).
10) G. Kamimoto, K. Teshima and M. Nishimura; Dept. Aero. Eng. Kyoto Univ. CP. no. 36 (1972).
11) P.H. Wojciechowski and H.D. Weymann; J. Chem. Phys. **61** 1369 (1974).
12) R.S. Giannaris and F.P. Incropera; J.Q.S.R.T. **13** 167 (1973).
13) D.R. Bates, A.E. Kingston and R.W.P. McWhirter: Proc. Roy. Soc. **A267** 297 (1962).
14) H. Shirai, K. Tabei and A. Kakinuma; Trans. Japan Soc. Aero. Sci. **21** 1 (1978).
15) J.P. Appleton and K.N. Bray; J. Fluid Mech. **20** 659 (1964).
16) M. Mitchner and C.H. Kruger; 'Partially Ionized Gases' John Wiley & Sons, Inc. (1973).
17) M.J. Seaton; 'Atomic and Molecular Processes' (ed. by D.R. Bates) 374 Academic Press Press (1962).
18) H. van Regemorter; Astrophysical J. **136** 906 (1962).
19) B.L. Moiseiwitsch and S.L. Smith; Rev. Mod. Phys. **40** 238 (1968).

20) H.W. Drawin; Z. Phys. **211** 404 (1968).
21) H.W. Drawin and F. Emard; Phys. Letters **43A** 333 (1973).
22) W.L. Wiese, M.W. Smith and B.W. Miles; 'Atomic Transition Probabilities' vol. II, NBS 22 (1969).
23) D.R. Bates and A. Damgaard; Phil. Trans. Roy. Soc. **A242** 101 (1947).
24) H.R. Griem; 'Plasma Spectroscopy' McGraw-Hill Book Co. (1964).
25) K.P. Horn; 'Radiative Behavior of Shock Generated Argon Plasma Flows' Stanford Univ. SUDAAR 268 (1966).
26) C.F. Hansen and R.L. McKenzie; J.Q.R.S.T. **11** 349 (1971).
27) M. Baranger; 'Atomic and Molecular Processes' (ed. by D.R. Bates) 493 Academic Press (1962).
28) H.R. Griem; 'Spectral Line Broadening by Plasmas' Academic Press (1966).
29) H.R. Griem, M. Baranger, A.C. Kolb and G. Oertel; Phy. Rev. **125** 177 (1962).
30) Ya.B. Zel'dovich and Yu.P. Raizer; 'Physics of Shock Waves and High-Temperature Hydrodynamic Phenomena' vol. I, Academic Press (1966).
31) D.R. Kennedy and S.T. Manson; Phys. Rev. **A5** 227 (1972).
32) A. Burgess and M.J. Seaton; M.N.R.A.S. **120** 121 (1960).
33) A.N. Belozerov and R.M. Measures; J. Fluid Mech. **36** 695 (1969).
34) J. Pomerantz; J.Q.S.R.T. **1** 185 (1961).
35) R.S. Devoto; Phys. Fluids **10** 354 (1967).
36) Y. Enomoto; J. Phys. Soc. Japan **35** 1228 (1973).
37) P.B. Coates and A.G. Gaydon; Proc. Roy. Soc. **A293** 452 (1966).
38) T.R. Carson; J.Q.S.R.T. **6** 563 (1966).